Acta Materialia 232 (2022) 117939

Contents lists available at ScienceDirect

Acta Materialia

journal homepage: www.elsevier.com/locate/actamat

Tuning mechanical properties of ultrafine-grained tungsten by manipulating grain boundary chemistry

Michael Wurmshuber[a,*], Severin Jakob[b], Simon Doppermann[a], Stefan Wurster[c], Rishi Bodlos[d], Lorenz Romaner[b], Verena Maier-Kiener[b], Daniel Kiener[a]

[a] Department Materials Science, Chair of Materials Physics, Montanuniversität Leoben, Jahnstraße 12, Leoben 8700, Austria
[b] Department Materials Science, Chair of Physical Metallurgy and Metallic Materials, Montanuniversität Leoben, Roseggerstraße 12, Leoben 8700, Austria
[c] Erich-Schmid Institute of Materials Science, Austrian Academy of Sciences, Jahnstraße 12, Leoben 8700, Austria
[d] Materials Center Leoben GmbH, Roseggerstraße 12, Leoben 8700, Austria

ARTICLE INFO

Article history:
Received 17 December 2021
Revised 21 March 2022
Accepted 11 April 2022
Available online 19 April 2022

Keywords:
Tungsten
Grain boundary segregation engineering
Ultrafine-grained metals
Smallscale testing
Nanoindentation
Atom probe tomography
Mechanical properties

ABSTRACT

Tungsten is, due to a combination of high strength and good physical properties, frequently considered for high-performance applications in the harshest environments. Oftentimes its inherent brittleness and low ductility stand in the way of a successful deployment in these fields. Since tungsten has been proposed as divertor material for nuclear fusion reactors, an improvement of ductility and fracture toughness is essential. An obvious first step to increase these properties is to reduce the grain size to the ultrafine-grained regime. As this still leaves the material with a relatively low-energy intercrystalline fracture mode, this work takes a step further. With the help of doping elements, which are identified from ab-initio simulations, an attempt to increase grain boundary cohesion of ultra-fine grained tungsten to improve ductility is made. After fabrication of the doped samples from powders using severe plastic deformation, thorough microstructural investigations and extensive mechanical characterization, utilizing various small-scale testing techniques, are combined to assess the properties of the materials. We report that the addition of boron and hafnium can significantly increase the bending strength and bending ductility of ultra-fine grained tungsten. An additional heat treatment of the boron doped sample amplifies this effect even further, drastically increasing the strength and overall mechanical properties due to a combination of hardening-by-annealing and increased grain boundary segregation. Thus, an effective way to adaptively improve the mechanical properties of tungsten by manipulating grain boundary chemistry is reported, validating grain boundary segregation engineering as a powerful tool for enhancing damage tolerance in brittle materials.

1. Introduction

Since the beginning of systematic materials science, researchers dream of a material that combines the “trinity” of mechanical properties: high strength, high ductility and enhanced fracture toughness. Especially ultra-high strength materials often cannot unleash their full potential, as they lack the ability to absorb damage from overloading or tolerate pre-existing defects within the material. The mutual exclusivity of strength and ductility in homogeneous metals has its roots in dislocation plasticity. As most strengthening mechanisms are based on restricting dislocation movement, this in turn deteriorates plastic deformation and ductility. Similarly, such strengthening mechanisms have a detrimental effect on fracture toughness, as the ability to successfully dissipate stress intensity from the crack tip via nucleation and propagation of dislocations is restricted [1]. The strength-ductility trade-off can, however, be challenged by implementing various strategies explored in recent years [1,2,11–13,3–10]. A reduction in grain size of metals, for example, commonly leads to an increase in strength [14,15] and fracture properties [16–18], while having little influence on the ductility. In fact, for coarse-grained metals sometimes even an increase in ductility can be observed, as the larger amount of grains gives a higher probability of dislocation slip systems being orientated beneficial to mechanical loading [2]. However, when entering the nanocrystalline regime (nc; grain sizes < 100 nm), the transition from a dislocation-controlled plasticity to a grain boundary (GB)-controlled plasticity leads to a strong decrease in ductility [2,3,7,19], with only a few fcc materials being able to retain their ductility through GB sliding and superplasticity [20–22]. Sim-

* Corresponding author.
E-mail address: michael.wurmshuber@unileoben.ac.at (M. Wurmshuber).

https://doi.org/10.1016/j.actamat.2022.117939

ilarly, the vast amount of GBs present in such small grained metals renders a comparably easy path for crack propagation, hindering fracture toughness to improve further [18,23]. Therefore, ultrafine-grained (ufg; grain sizes between 100 and 500 nm) materials seem to represent a favorable tradeoff to achieve ultra-high strength, decent fracture toughness and still acceptable ductility.

Due to the large amount of GBs in ultra-fine grained materials, GB cohesion is of great significance for the mechanical performance. As mentioned above, grain boundaries are usually the weak link in ufg and nc materials. Therefore, in order to reinforce these weak spots, the concept of grain boundary segregation engineering (GBSE) has been introduced [24,25,34,35,26–33]. In GBSE, materials that are known to break in an intercrystalline fashion are doped with elements that are predicted to strengthen GB cohesion. By heat treatments or mechanical mixing, these elements, e.g. boron in steels [36], segregate at the GB for an optimal GB strengthening effect. A related approach, the avoidance or removal of segregation of GB embrittling elements, such as S, P or O, has been practiced ever since medieval times and is an important first step to enhancing GB cohesion [37]. The process of identifying GB strengthening elements in a given host material has been supported in recent years by ab-initio simulations, such as density-functional theory [26,29,42–44,32,33,35,36,38–41].

Tungsten has been considered a promising structural material for the divertor part in nuclear fusion reactors, due to its unique properties such as high strength, high melting point, excellent thermal conductivity, outstanding erosion resistance and its small tendency to become activated or transmuted [45–49]. As a refractory metal, it also shows inherent brittleness and intercrystalline fracture even for conventional grain sizes, which is the major concern for employment of tungsten materials in the harsh environment of nuclear fusion reactors as of today [45,46,55,47–54]. By reducing the grain size of tungsten down to the ufg regime, it could not only gain a valuable increase in strength and fracture toughness [8,10], the large fraction of GBs introduced would also prove themselves beneficial for counteracting and absorbing radiation damage [56–62] and for suppressing the growth of helium bubbles, an unavoidable by-product of the fusion reaction [63–67]. Grain refinement in combination with GBSE is therefore a promising approach to improve the mechanical properties of tungsten and create a material showing an excellent combination of strength, ductility and toughness, even in harsh environments. In this work, several ufg W samples, undoped and doped with various atomic elements, are fabricated using severe plastic deformation. Utilizing extensive microstructural and mechanical characterization, the direct effect of each doping element on the mechanical properties of ufg tungsten is identified and interpreted.

2. Experimental methodology

2.1. Material and fabrication

To enhance the grain boundary cohesion in ufg W, several elements have been chosen as candidate doping elements, based on the ab-initio simulations of Scheiber et al. [38,39]. Disregarding elements that form brittle intermetallic phases in tungsten, are toxic or not affordable for a potential large scale fabrication in the future, the four elements carbon, boron, rhenium and hafnium were selected in this work. It should be noted that, according to [39], Hf does not strengthen the GB cohesion directly. While a different work by Setyawan et al. [40] suggests that Hf could possibly strengthen the grain boundaries in a tungsten host material, in this work it was mainly chosen due to its well-known affinity to oxygen. As oxygen located at GBs is considered as a main contributor to the brittleness of tungsten [38,49,68], it is presumed that Hf as doping element will bind oxygen in the form of hafnium oxide and therefore remove it from the grain boundaries. This strategy has already been applied successfully in previous work on molybdenum [31]. Notably, to ensure their targeted deployment, all selected doping elements show an increased GB segregation tendency in W [38,39].

A fabrication route for ufg W from elemental powders using high pressure torsion (HPT) has been developed by the authors in a previous work [69]. The advantage of starting from powders is the ability to precisely control chemical composition in terms of doping with impurity and alloying elements. The material powders of W (99.97% purity, 2 µm particle size, Plansee SE, Austria), C (99.95% purity, 2 – 12 µm particle size, Merck KGaA, Germany), B (98% purity, 44 µm particle size, Alfa Aesar, USA), Re (99.99% purity, 10 µm particle size, Mateck GmbH, Germany) and Hf (99.6% purity, 44 µm particle size, Alfa Aesar, USA) are all stored and handled in argon atmosphere within a glovebox. The powders are mixed to adjust the content of the doping element at approximately 3 – 5 at.%. Subsequently, the powder mixtures are compacted in argon atmosphere using a sealed mini-chamber [69] and a high pressure torsion tool [70]. A nominal pressure of 12 GPa and torsional deformation of about 0.1 rotations are applied to the powders. After the powder is compacted, an intermediate annealing step at 1600 °C for 7 hours in a vacuum furnace (Leybold Heraeus PD 1000, Leybold GmbH, Germany) is performed to enhance powder particle cohesion. Finally, the samples are deformed using HPT with a nominal pressure of 12 GPa at 400 °C for about 1 rotation, resulting in disk shaped specimens with a diameter of 6 mm and a height of 0.6 – 0.8 mm. For more detailed information regarding the fabrication route of the ufg W samples, the interested reader is referred to [69].

Following the results of mechanical property tests presented in Section 3,an undoped and a boron-doped ufg W sample were heat treated at 500 °C for 5 hours in a vacuum furnace (XERION Berlin Laboratories GmbH, Germany) subsequent to the HPT deformation with the intention to increase grain boundary relaxation and doping element segregation. The annealed samples are marked with “ann.” in all Figures in this work.

2.2. Microstructural characterization

The microstructures of the samples were investigated using a field-emission scanning electron microscope (SEM; LEO type 1525, Zeiss GmbH, Germany) equipped with energy dispersive X-ray spectroscopy (EDX; Bruker XFlash 6|60, Bruker, Bruker Corp., USA) and electron backscatter diffraction (EBSD; Bruker e$^-$-Flash^{FS}, Bruker Corp., USA) detectors. In order to assess the GB chemistry via atom probe tomography (APT), lift-outs of selected samples were fabricated using an Omniprobe 200 manipulator (Oxford Instruments plc, UK) in a dual-beam focused ion beam (FIB)-SEM (Zeiss Auriga, Zeiss GmbH, Germany). From the lift-outs, APT tips containing GBs were fabricated following the procedure detailed in [71] on an FEI 3D DualBeam workstation (Thermo Fisher Scientific, USA) equipped with an EDAX Hikari XP EBSD-system (AMATEK Inc., USA). The APT experiments were performed on a CAMECA LEAP 3000HR (AMATEK Inc., USA) in laser-pulse mode with a laser energy of 0.6 nJ at 250 kHz, a test temperature of 60 K and a target evaporation set to 0.5%. The software IVAS 3.6.14 was used for the reconstruction and analysis of the measured atom probe tips.

2.3. Indentation

In order to get a first assessment of mechanical properties of the produced samples, Vickers microhardness was measured along the sample radius in tangential direction with a load of 500 g using a Buehler Micromet 5104 machine (Buehler ITW Test & Measurement GmbH, Germany). In-depth information about mechani-

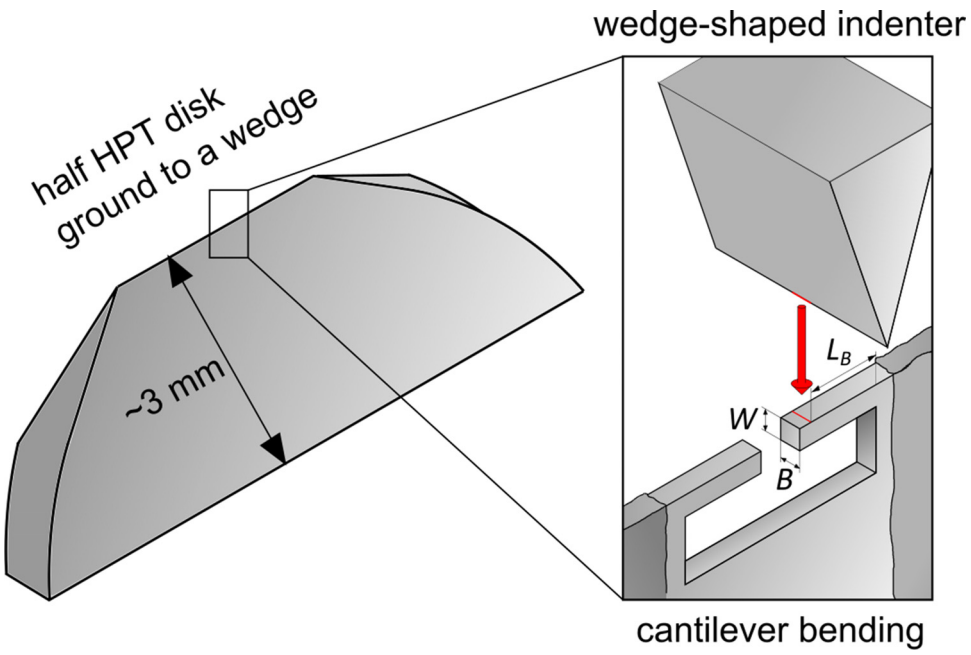

Fig. 1. Micromechanical testing setup for microcantilever bending.

cal properties, such as strain-rate sensitivity (SRS) or activation volume, was acquired by performing strain-rate jump tests [72,73] using a G200 Nanoindenter (KLA Corporation, USA) equipped with a diamond Berkovich tip and the continuous stiffness measurement (CSM) option. A minimum of four tests were performed at a sample radius of 3 mm for each material condition.

2.4. Microcantilever bending tests

As the HPT process leads to a deformation gradient, and consequently also a microstructural gradient, along the sample radius, the smallest and most desired grain size is usually found in the outer region of the sample disk. To only test this specific microstructure and avoid unintended influences from the coarser grained regions at smaller radii, small-scale testing techniques are necessary to specifically probe the mechanical properties of ufg W.

For the most crucial assessment of the mechanical performance of tungsten, samples should be loaded under tensile stress conditions. However, microtensile tests are demanding in sample preparation and unforgiving in terms of alignment [74–80]. Additionally, it is challenging to find a suitable gripper material stiff and hard enough to test the samples produced in this work. As most available grippers for tensile testing are made of tungsten themselves, it is likely that plastic deformation will also occur in the gripper during the experiment, damaging the gripper and distorting the recorded force-displacement data [80].

Therefore, in an attempt to combine (partial) tensile testing conditions and practicability in unveiling mechanical properties and deformation behavior of the doped and undoped ufg W samples, microcantilever bending tests were performed. For this, the as-deformed HPT disks are cut in half using a diamond wire saw and then ground to a wedge shape using a special sample holder. From the very top of the wedge, cantilevers with dimensions of about 3 × 3 × 10 µm are fabricated using a dual-beam FIB-SEM (Zeiss Leo 1540XB, Zeiss GmbH, Germany), as depicted in Fig. 1. The cantilevers are tested in-situ in a field-emission SEM (Zeiss LEO 982, Zeiss GmbH, Germany) using an UNAT-SEM indenter (Zwick GmbH & Co KG, Germany) equipped with a conductive diamond wedge indenter tip (Synton-MDP AG, Switzerland). The recorded force and displacement data, can be converted to bending stress and bending strain, respectively, using the following equations [81–83]:

$$\sigma_{max,tensile} = 4 \cdot \frac{F \cdot L_B}{B \cdot W^2} \tag{1}$$

$$\varepsilon_{max,\ tensile} = \frac{3 \cdot W \cdot u}{2 \cdot {L_B}^2} \tag{2}$$

where $\sigma_{max,tensile}$ and $\varepsilon_{max,\ tensile}$ are the maximum tensile stress and tensile strain at the outermost fiber of the cantilever, respectively, F is the load, u the displacement, L_B the bending length, B the width and W the thickness of the cantilever (compare with Fig. 1). The displacement rate for these experiments was set to 20 nm/s, which corresponds to a strain rate of $\sim 10^{-3}$ s^{-1}. In-situ videos of all experiments were compiled by collecting an image of the SEM screen every second. For each material condition 3-4 cantilevers were fabricated and at least 2 were successfully tested.

3. Results

3.1. Microstructure and grain boundary chemistry

SEM images of the microstructure of the as-deformed undoped and doped ufg W samples are displayed in Fig. 2. All images were taken at a radius of 3 mm from the disk center in tangential direction. The grain sizes were measured using the grain intercept method. As apparent in Fig. 2, the microstructures for all produced samples are rather similar, the measured grain sizes confirm this assumption with all of them lying in the range of 110 – 160 nm. It should also be noted that – as intended – the heat treatment of an undoped and a boron doped specimen did not lead to any noticeable grain growth. As is apparent in lower magnification overview pictures (Fig. 3), the formation of various up to several micron-sized particles was observed in the final microstructure of the doped materials. The formation of HfO_2 oxides in the hafnium-doped sample was expected and desired and the formation of WB borides can be easily explained by the large negative mixing enthalpy of B and W [84] in combination with the high shear strain present during HPT processing. The formation of the other large particles, on the contrary, is rather surprising. The W_2C carbide

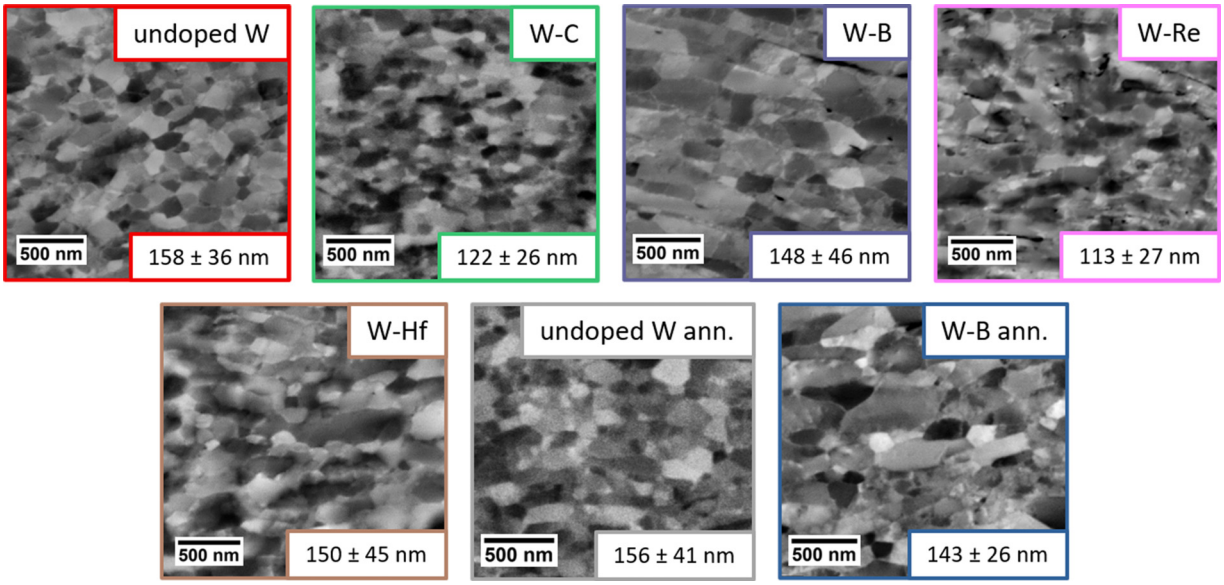

Fig. 2. SEM microstructure images and grain sizes of all investigated W materials. Images were taken using a backscattered electron detector at a sample radius of 3 mm in tangential direction. Samples marked with "ann." underwent a heat treatment at 500 °C for 5h in vacuum after HPT deformation.

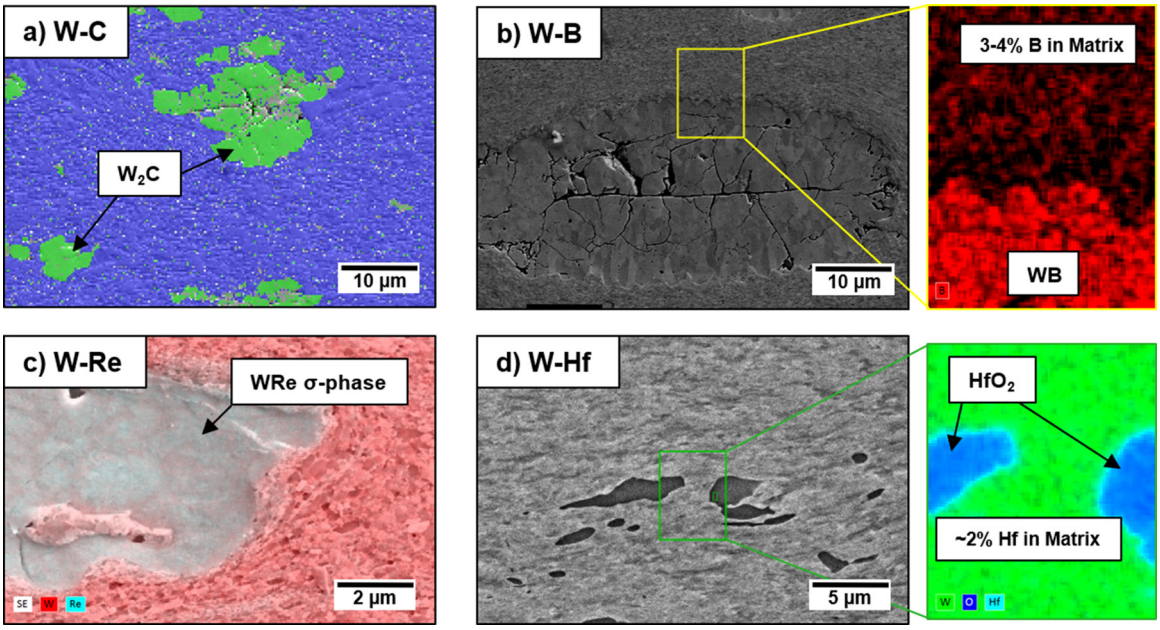

Fig. 3. Lower magnification micrographs revealing various particles formed through HPT. a) EBSD map of carbon doped sample with metastable W_2C carbides. b) SEM image and EDX map of boron doped sample with WB borides. c) EDX map of rhenium doped sample with WRe intermetallic σ-phase. d) SEM image and EDX map of hafnium doped sample with HfO_2 oxides.

should not be stable below 1200 °C under equilibrium conditions according to the phase diagram and the formation of WRe intermetallic phase contradicts the well-known high solubility of Re in W [85]. It is assumed that, due to the metastable nature of some of the phases, these particles form through intimate mixing originating from the high pressure and shear strain during the HPT-deformation [86,87], yet their exact origin is not fully clear and will be subject to future work. As EDX measurements revealed that there is still enough concentration (2 – 4 at.%) of the doping elements in the W matrix, and it is relatively easy to avoid them when fabricating micromechanical specimens, the particles do not influence the outcome of the present small-scale testing experiments (with the exception of the HfO_2 oxides, which are supposed to remove and bind pre-existing oxygen from the GBs).

To explore the segregation behavior of B, undoped W, W-B and heat treated W-B samples were additionally investigated regarding their GB chemistry using APT. The samples doped with B were chosen as representative APT samples, due to the difficulties of measuring B with EDX and because of the clear improvement of mechanical properties of ufg W by doping with B, as presented in section 3c. The results from these measurements are depicted in Fig. 4. For every material condition, a tip containing a vertical grain boundary was selected for analysis and detailed investigation. The presence of a GB is indicated by the different Ga-content (Fig. 4**a**), W isosurfaces (Fig. 4**c**) as well as the respective region of interests for GB analysis. The undoped W sample shows no significant segregation of any elements along the GB, with the exception of Ga, which is unavoidable to be introduced into the material dur-

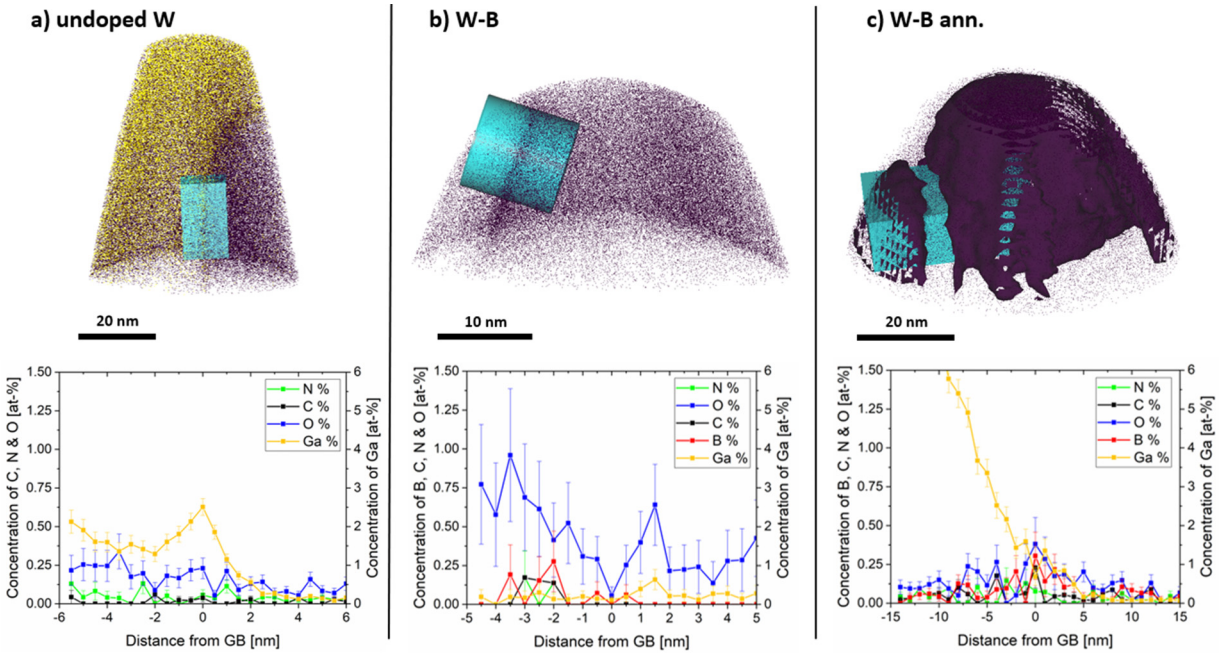

Fig. 4. APT tips and investigations of element segregation at the GB in a) undoped W, b) W-B and c) annealed W-B samples.

ing FIB preparation. The unannealed boron doped specimen also shows signs of Ga and only a small amount of B inside the material. This indicates that the B must be very finely distributed within the sample and not segregated at the GB. After a heat treatment at 500 °C for 5 hours, segregation of about 0.3 at% B in the 1D-concentration profile was detected at the GB of the material (see Fig. 4**c**). The interfacial excess value for B was calculated according to [88,89] and amounts to 0.23 at/nm². Oxygen was identified to some extent in all investigated APT specimen at and near the GB.

3.2. Hardness and strain-rate sensitivity

Fig. 5**a** shows the hardness along the sample diameter for all samples. A clear gradient in hardness, originating from the deformation gradient of the torsion deformation, is apparent. It seems that the two interstitial doping elements, C and B, lead to slightly higher hardness in the inner regions of the disks. However, at a distance of about 3 mm from the disk center, where all further experiments in this work will be performed at, the hardness values all lie in a range of 800 – 1000 HV0.5 (grey shaded area in Fig. 5**a**). The undoped annealed sample broke during sample preparation, which is the reason for not testing the whole specimen.

Results from strain-rate jump tests are visible in Figs. 5**b** and 5**c**. The SRS coefficient and the activation volume were analyzed following the procedure of Maier-Kiener et al. [72,73]. It is apparent that the values are comparable, around 0.013 - 0.017 for SRS and 7-9 b³ in activation volume, with the exception of W-Re that showed a reduced SRS of 0.010 and increased activation volume of ~13 b³.

3.3. Microcantilever bending

A representative stress-strain curve ($\sigma_{max,tensile}$ - $\varepsilon_{max,\ tensile}$, see Equations (1), (2)) for the boron doped sample including snapshots from the in-situ SEM video of the respective cantilever test is depicted in Fig. 6. As there is no standard procedure for extracting material properties out of bending stress - bending strain curves, the following parameters were used in this work to compare the different materials: As a measure of strength, the maximum bending stress recorded in the experiments was used. This serves as an equivalent to a UTS value and was deemed to be the most reasonable quantity to compare. Obtaining a measure of ductility from the bending curves is a more challenging task. As all experiments are performed in-situ in an SEM, one can utilize the available video information for that. The point in the video of each tested cantilever that shows first signs of crack formation was correlated with the stress - strain curve. The plastic strain at this point (i.e. total strain minus elastic strain) is used as a measure to compare ductility of the tested samples. A drawback of this method is, that through the in-situ pictures we only gain information of one side of the tested cantilevers, thereby possibly overlooking crack formation on the backside of the specimen. However, due to the small cantilever dimensions, it is likely that such a crack would be visible on the observed side shortly after, in which case only a minimal error in ductility is made. Moreover, for the presented experiments whenever there was a sudden load drop in the recorded curves, this point was set as default failure event, and – most importantly – always coincided with visible crack formation. Out of these reasons and in the absence of a better alternative, this measure of ductility was defined. It should, however, be clear that this is not to be regarded as a one-to-one equivalent to tensile ductility. Cantilevers that have been found to contain visible cracks or pores in or near the bending area have been discarded already before testing.

A compiled “strength - ductility map” of all fabricated material samples is shown in Fig. 7**a**. It is no surprise that the strength of all tested materials lies well within the ultra-high strength regime, given the immense intrinsical strength of the tungsten base material combined with an ultra-fine grain size. All tested unannealed samples show strengths exceeding 2500 MPa up to 4500 MPa. The ductility ranges from rather small failure strains of 2.5% to strains of 15%, which is very respectable for such a high strength material. It is noteworthy that, with the exception of C, all doping elements increase the strength of ufg W, while only two of them, B and Hf, also maintain or improve ductility. The positive effect of B and Hf is further underlined in Fig. 7**b**, where the area below the stress-strain curves until failure, i.e. the plastic work of the material or plastic energy density, are shown. Values of 406 ± 5 MJ/m³ (boron)

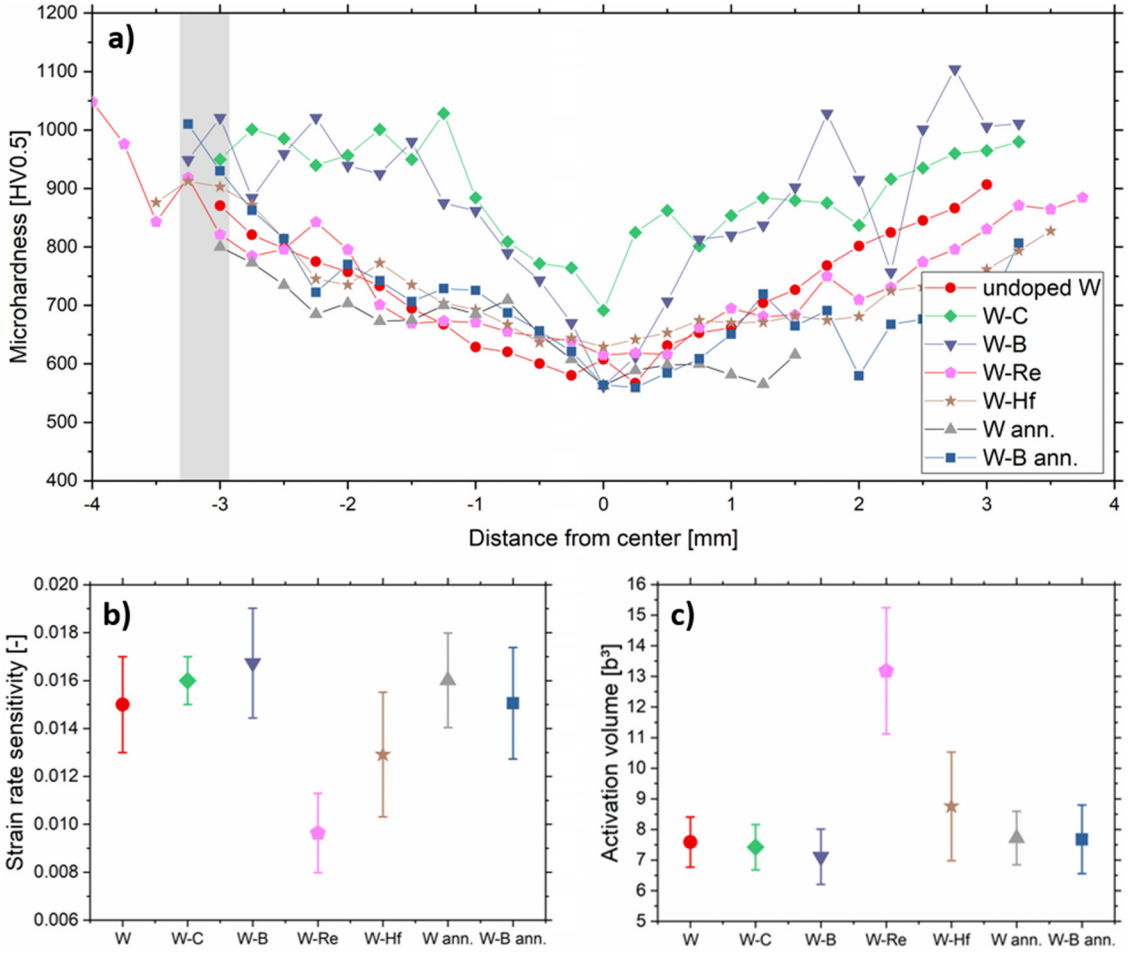

Fig. 5. Indentation results of all investigated W samples. a) Microhardness across the diameter of the HPT disks. The grey shaded area marks the region on the samples, where all further experiments are performed. b) SRS and c) activation volume results from nanoindentation strain-rate jump tests.

and 363 ± 14 MJ/m³ (hafnium) are a clear improvement compared to the undoped material (286 ± 21 MJ/m³). In Fig. 7 it is also apparent that doping with C deteriorates the mechanical properties of ufg W, even though Scheiber et al. [38] predicted it to be a GB strengthening element in tungsten, and the beneficial effect was demonstrated in Mo [31].

Following the great performance of the B doped ufg W sample, this material was additionally heat treated at 500 °C to deliberately enhance the GB segregation of the doping element. The undoped ufg W was also annealed at the same conditions to provide a reference sample. As is apparent in Fig. 7**a**, the annealed samples show an enormous increase in strength compared to all other tested samples. The strength of the undoped and annealed W material is 5.37 ± 0.25 GPa, whereas the annealed W-B material displays an even higher strength of 7.08 ± 0.33 GPa, more than double the strength of the undoped and unannealed W material (3.28 ± 0.37 GPa). Moreover, the ductility of the annealed samples (8.3 ± 2.8 % and 8.2 ± 2.2 %, respectively) is comparable with the unannealed undoped W (8.7 ± 0.8 %) and unannealed W-B samples (8.9 ± 0.3 %). By maintaining ductility while at the same time drastically raising the strength, the overall spent plastic work also increases dramatically to 450 ± 130 MJ/m³ and 658 ± 224 MJ/m³, respectively, as can be observed in Fig. 7**b**.

4. Discussion

The fabrication route presented in [69] and applied in this work was found to be successful in reliably processing tungsten powders to dense bulk samples of ultra-fine grain size in the range of 110-160 nm (Fig. 2). These ufg samples do not only excel on their own in terms of high strength and noticeable ductility, the powder fabrication route also allows for precise doping with GB strengthening elements to enhance these properties even further.

As revealed by APT measurements on the boron-doped sample (Fig. 4), respective doping elements are not primarily situated at the GB, which is not too surprising as their distribution is achieved by mechanical deformation with only little thermal input. Only an additional heat treatment provides the necessary energy for the doping elements to diffuse towards and segregate at the GBs. From the presented APT results, it is safe to assume that before such a heat treatment, the doping elements are randomly distributed within the material, as an enhanced GB segregation tendency is thermodynamically given [38,39], but kinetically limited.

While the hardness results (Fig. 5**a**) might indicate that the interstitial doping elements C and B lead to higher hardness, a more reasonable explanation for the bulk hardness increase is the formation of µm-sized and extremely hard W_2C carbides and WB borides, as seen in Fig. 3**a** and 3**b**. Remember that carbides and borides were avoided for microcantilever testing. While there are also HfO_2 oxides and WRe intermetallic phases found in the other fabricated samples (Fig. 3**c** and 3**d**), those are smaller in size and amount and assumed to be softer than the borides and carbides. As such, only for the carbides and borides a noticeable increase in bulk hardness was observed. At the edge of the disk specimen, where all further experiments were conducted, the hardness of all samples lies in the same range of 800 - 1000 HV0.5, so no

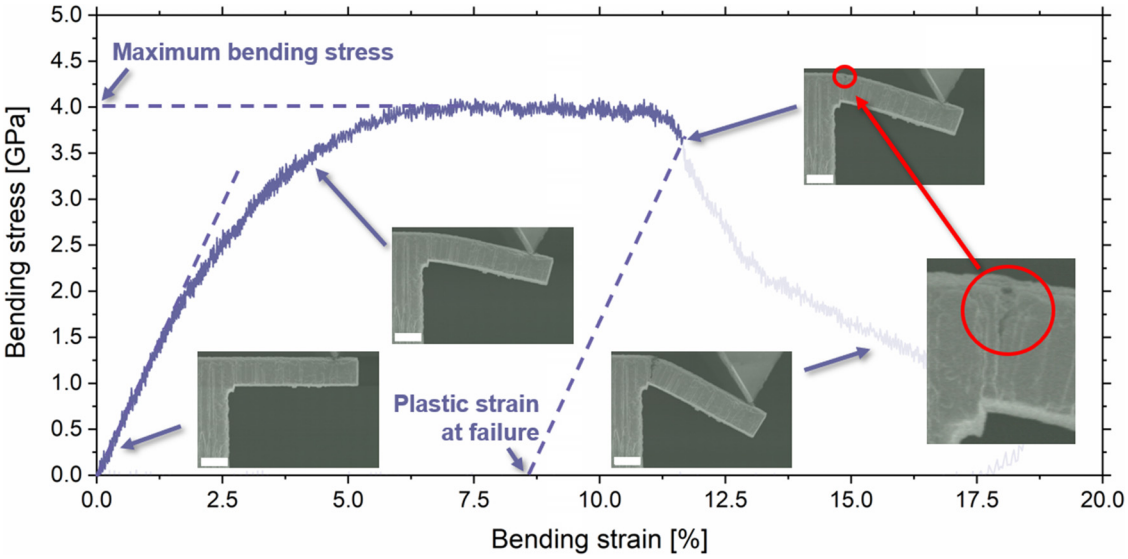

Fig. 6. Representative stress-strain curve of boron doped ufg tungsten and in-situ pictures of the respective bending test. The white scale bars in the lower left of the in-situ pictures represent a length of 2 µm.

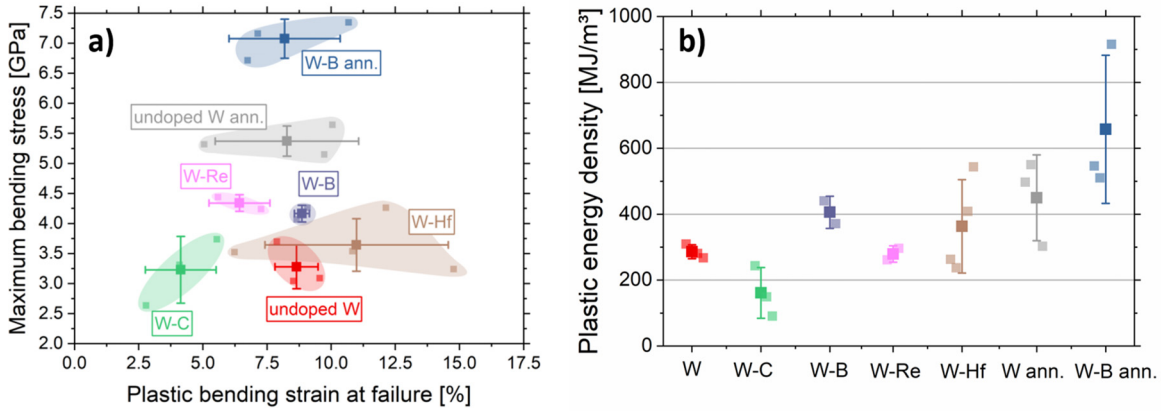

Fig. 7. a) Maximum bending stress (i.e. strength) over plastic bending strain at failure (i.e. ductility) of all fabricated materials. Each small square represents a successful microcantilever bending test, the big squares represent the average strength and ductility of each material. b) The integrated area below the stress-strain curves until failure is taken as a measure for plastic work expended during deformation for all fabricated samples.

significant change related to the doping elements is observed here. Furthermore, the annealed samples show a similar hardness distribution as the ufg W variants doped with substitutional elements or the undoped material. This confirms that no significant grain growth occurred during the annealing. It should be mentioned that the annealed W-B sample shows lower hardness than the unannealed W-B material in the inner regions of the sample disks. This can be explained by dislocation recovery phenomena in these coarser grained regions, which are known to onset in cold-worked W at about 400 °C [90].

The SRS and activation volumes probed by nanoindentation strain-rate jump tests (Fig. 5**c**) lie in a range of 0.013 - 0.017 and 7-9 b^3, respectively, which is commonly attributed to the kink-pair mechanism regarded in bcc metals at low temperatures [91–97]. Here, the rhenium doped sample shows a slightly higher activation volume and reduced SRS, which is in good agreement with the theory that Re promotes dislocation glide in tungsten by altering the asymmetry of the screw dislocation core [98]. Annealing the W and W-B samples leads to no obvious change in SRS and activation volume, indicating once again that no major microstructural changes are taking place during the heat treatment, except for the intended B diffusion and segregation.

While the doping elements seem to only have a minor influence on GB mobility and thus resulting grain size as well as hardness and activation volume, the results from microcantilever bending tests paint a different picture. Due to the partial tensile nature of the bending test, the most crucial loading mode for tungsten is tested. Therefore, any influence of a modified GB cohesion would show the biggest effect in these tests. Before discussing the results of the microbending tests, it should be mentioned that the cantilevers were examined with the crack growth direction in radial specimen orientation. To demonstrate the influence of this test orientation on the mechanical properties, further microstructural analysis has been performed. Fig. 8**a** and 8**b** show the cumulative grain size distribution in axial and radial direction, respectively. From this data it can be seen that the grain size distribution is relatively slim, indicating a uniform grain size in the respective directions. However, it is also apparent that the average grain size in axial direction is smaller than in radial direction. This grain anisotropy is further visualized in Fig. 8**c**. The grain aspect ratio of all investigated ufg W samples lies between 1:1 and 1:2, with the majority of samples showing a ratio close to 1:1.5. As demonstrated in previous work [99,100], this slight grain shape anisotropy originating from the torsional deformation leads to an

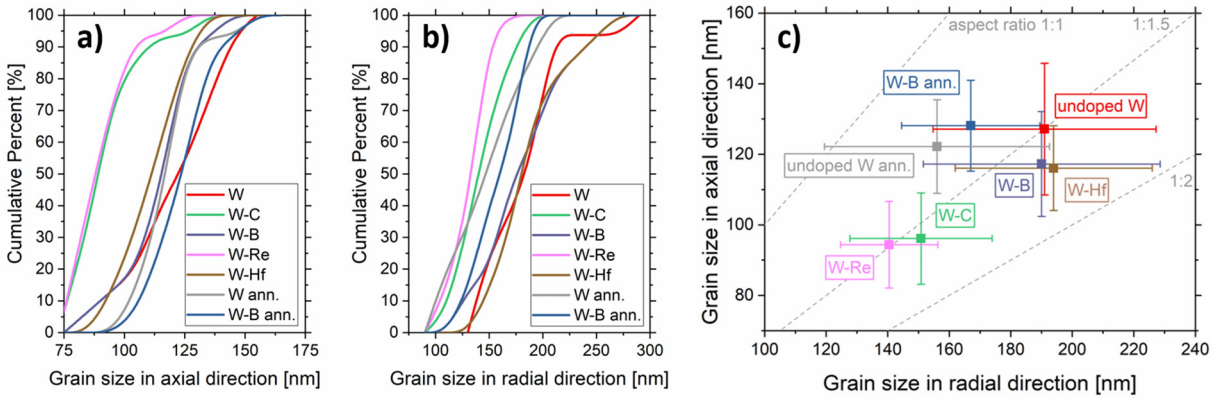

Fig. 8. Cumulative grain size distribution of grains in a) axial and b) radial direction of all investigated samples. c) Grain anisotropy of axial and radial direction show an aspect ratio of 1:1.5 for most ufg W samples.

orientation dependence of fracture performance for HPT processed ufg materials. The configuration used in the present work, with the crack growth direction in radial specimen direction, was found to yield the highest fracture toughness values. As intercrystalline fracture is also a major factor controlling ductility in such an ultra-fine grained material, a similar directional dependence is assumed for ductility. However, since grain shape and anisotropy could potentially be tuned by larger scale fabrication methods (e.g. rolling) and aligning the microstructure in a preferred loading direction is usually possible, the authors decided it is best to test the material in this direction to show the potential of the material, rather than testing a potentially weaker direction.

The microcantilever bending results in Fig. 7**a** underline that ufg W shows very attractive mechanical properties. The undoped material already demonstrates a strength of 3.28 ± 0.37 GPa, higher than cold-rolled tungsten [101], highest-strength steels [102,103] or previous works on ufg W [94,104], while also exhibiting a formidable bending ductility of 8.7 ± 0.8 %, unprecedented in tungsten [49,101]. Notably, as the stress and strain distribution is much more complex for a bending experiment than for a tensile experiment, we do not advise to directly compare the strength and ductility values gained in this work with tensile or compression values in literature. That being said, as the nature of the experiment still yields a valid stress-strain curve, the feasibility to compare the strength and ductility for materials tested in the same bending test conditions, and therefore the ability to correctly assess the effect of each doping element on strength and ductility, prevails.

From the EBSD images in Fig. 9**a** and 9**b**, it is apparent that the undoped W cantilevers fail – as expected – in an intercrystalline fashion, since the grains on either side of the crack have different orientations. This is crucial, as an improvement of mechanical properties by GBSE can only be expected when the failure mode is in fact intergranular. All tested ufg W variants failed intergranularly, as is evident by EBSD images on a representative annealed W-B cantilever shown in Fig. 9**c** and 9**d**. The profiles of the crack onset and fracture surfaces seen in top view SEM micrographs of annealed undoped W (Fig. 9**e**) and annealed B doped W (Fig. 9**f**) provide additional evidence for intercrystalline failure in the materials.

Figs. 9**e** and 9**f** also show that there is no pronounced necking in the gauge area of the cantilevers, indicating homogenous deformation. In fact, the transverse strain measured in all cantilevers never exceeded 2.3%. When accounting for this strain using a Mohr's strain circle, a maximum relative error of $< 3\%$ is made for ductility, which corresponds to a maximum absolute error in failure strain of 0.3% (percentage points) for a worst case scenario. Therefore it is safe to assume that the cantilevers show predominantly homogeneous deformation in the bending area, justifying the chosen testing method for strength and ductility.

By adding the targeted doping elements to ufg W and conducting heat treatments, different effects on strength and ductility can be observed, which are outlined and discussed individually below:

4.1. The effect of annealing

As showcased by the undoped annealed sample, a moderate heat treatment at 500 °C for 5 hours enhances the strength of the material, while preserving the microstructure. This adaptive strength increase can be explained by the hardening-by-annealing effect, a phenomenon commonly found in very fine grained metals [105–109]. By annealing nc and ufg materials below the grain growth threshold temperature, on the one hand mobile dislocations annihilate at GBs, and on the other hand GBs relax into an energetically more favorable state. In the case of severely plastically deformed materials, this relaxed GB state is usually associated with "smoother" GBs that do not contain many GB ledges or other GB defects which could serve as possible sources for easier dislocation nucleation [2,59,106,109–113]. By removing both, mobile dislocations in the grain interior and potential nucleation sites at GBs, plastic deformation could only occur through a limited amount of conventional dislocation sources in the grain interior or nucleation of dislocations at relatively smooth GBs, which requires a higher stress level compared to dislocation nucleation at GB ledges, therefore explaining the increase in strength. It should be noted that this hardening-by-annealing phenomenon does not seem to have an influence on ductility of ufg W, indicating that there is still sufficient dislocation plasticity present in the material and underlining once more that GB cohesion is the limiting factor to ductility. It is interesting to note that the hardening-by-annealing seems to have no influence on the measured microhardness of ufg W, as can be seen in Fig. 5. Considering that both the required stress level for dislocation nucleation from GBs as well as the type of nucleated dislocations are severely different between tensile and compressive loading conditions [114], this might be an indicator that tensile stress conditions are more sensitive to such a GB relaxation effect. Such a presumed scenario would bear critical implications, since most hardening-by-annealing studies are conducted using hardness measurements, but this requires further investigation to proof in detail.

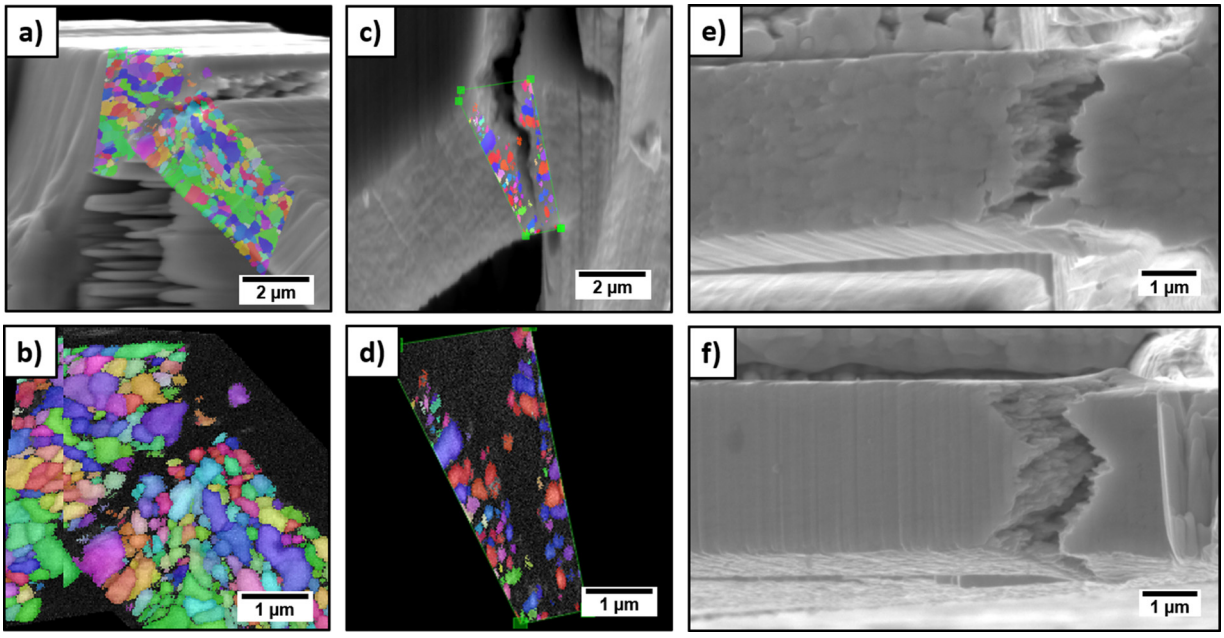

Fig. 9. EBSD overlay on SEM image of a) an undoped W and c) an annealed W-B cantilever after testing. b,d) Zoomed in EBSD maps around the crack, indicating intercrystalline failure. Top view SEM micrographs of annealed undoped W (e) and annealed B doped W (f) cantilever indicating predominantly homogeneous deformation in the gauge area and clear evidence of intercrystalline failure.

4.2. Carbon

The addition of C decreases ductility and, as a consequence, the overall plastic energy density (see Fig. 7**b**) of ufg W. Even though it has been identified as a GB cohesion enhancing element [38], such an effect could not be confirmed with the current testing efforts. C is known to change the core of screw dislocations in W and other bcc metals to a less mobile hard core configuration, limiting the ductility in a W-C solid solution [115–117], which would natively detoriate ductility. Another possible explanation for the reduction of mechanical properties might be the formation of nanosized carbides at the GBs, but within the present investigations we were not able to identify any. However, as doping of ufg W with C seems to not improve the bending stress-strain properties, this work aims its detailed attention at more promising variants instead.

4.3. Boron

Doping with B increases the strength and also slightly the ductility of ufg W. Therefore, also thespent plastic work and overall mechanical properties improve. As deduced from APT measurements and mentioned above, the B in this sample is most likely very finely and randomly distributed within the specimen, indicating that already a very small amount of B at the GB can improve the properties tremendously. Therefore, it is no surprise that an additional heat treatment, which promotes more segregation of B at the GB, amplifies this effect even further. As can be seen in Fig. 7**a**, the boron doped and annealed samples shows extraordinarily high strength values even exceeding 7 GPa. Furthermore, this incredible increase in strength is achieved while simultaneously maintaining the bending ductility at the same level as for the undoped W or unannealed W-B sample. Naturally, this increase in strength also leads to outstanding values for the plastic energy density of the material (Fig. 7**b**). This increase in mechanical performance is explained by a combination of three effects: 1) The above mentioned hardening-by-annealing effect leads to a strength increase on its own through GB relaxation and dislocation annihilation. 2) Moreover, out of all predicted elements within the simulations of Scheiber et al. [38,39], B showed one of the highest potentials for GB strengthening, making it a very potent GB cohesion enhancer, and 3) as an interstitial element with a high GB segregation tendency in W [38], boron could potentially remove and replace the weakening oxygen at the interstitial GB sites, thereby strengthening the GB both directly and indirectly (see Fig. 10). These combined positive aspects explain the highly effective property enhancement of B in annealed ufg W. The APT measurements in Fig. 4**b** are confirming that oxygen is depleted directly at the GB in the W-B sample. However, in the annealed material (Fig. 4**c**) a slight segregation of O is found in addition to the B segregation. This indicates that the strengthening effect of the segregated B is enough to completely outweigh the weakening effect that O has on GB cohesion.

4.4. Rhenium

The W-Re material showed an increase in strength but a slight decrease in ductility. This is surprising, as Re usually has the opposite effect in a W host material [85,97,98]. Considering the reduced SRS and increased activation volume values acquired by nanoindentation strain-rate jump tests, it is evident that Re has a positive effect on dislocation mobility [98,118], yet from the bending experiments it does not seem to be very potent in avoiding GB failure. While the ab-initio simulations in [39] predict Re to strengthen the GB cohesion in W, they also show that the effect of Re on the GB would only be about 20% compared to that of e.g. boron. We could rationalize this behavior by considering that higher dislocation mobility might promote pile-up formation at GBs, with the related stress localizations promoting grain boundary failure. However, as no clear improvements of the mechanical properties by doping with Re were observed (Fig. 7**b**) and Re is a rather expensive material, making it unattractive for future large scale fabrication and application, we do not follow this consideration up with detailed investigations, as this would require e.g. in-situ TEM studies.

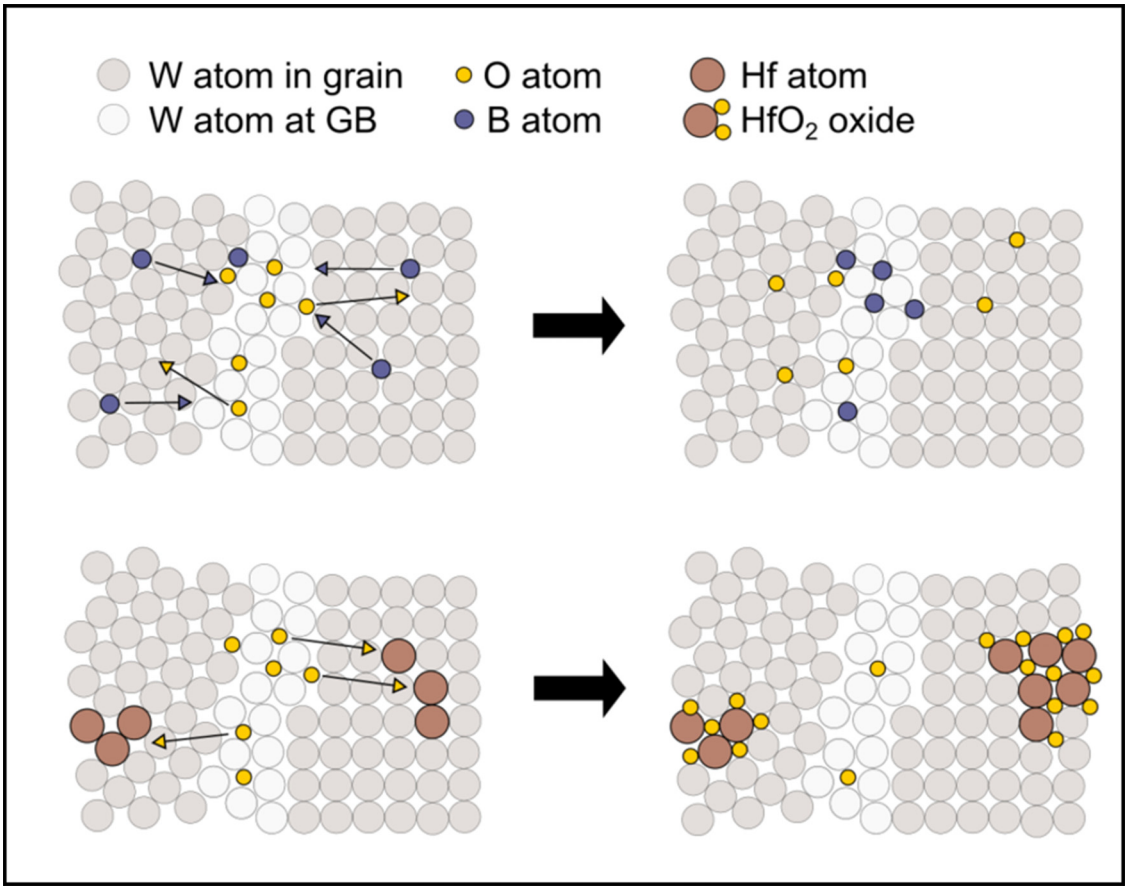

Fig. 10. Schematic of the effects of B and Hf on the GB chemistry. Boron diffuses to the GB and replaces O, while Hf attracts O from the GBs and forms HfO_2 oxides.

4.5. Hafnium

The hafnium doped sample shows improved strength and ductility, but also a large variability among the individual tested microcantilever. The well-known affinity of Hf to O and the observed formation of HfO_2 (Fig. 3**d**) leads to the conclusion that Hf is very effective in binding oxygen, therefore removing the embrittling element from the GB to indirectly strengthen GB cohesion in ufg W (see Fig. 10). This behavior has already been observed for Mo in the past [31]. While this effect is rather interesting and leads to a clear improvement of the mechanical properties, it is not evident that it can be further improved or utilized for an adaptive material characteristic, e.g. by forced segregation through annealing, since a direct strengthening effect of Hf at the GB is not likely [39,40] and the majority of oxygen is presumably already bound in the hafnium oxides. The large variation among the different W-Hf cantilevers, however, could be a sign of a varying effectivity of Hf in removing oxygen throughout the sample, indicating that more oxygen from the initial powder surfaces could potentially be bound either through diffusion by an annealing step or by initially adding more Hf to the powder mixture. Another possible explanation for the large variation among the cantilever properties could be undetected smaller HfO_2 particles within the cantilevers, reducing the probed ductility.

Finally, as B and Hf show the most promising improvement of mechanical properties of ufg W and the material is potentially interesting for employment in nuclear fusion reactors, the behavior of the two doping elements under irradiation should be briefly discussed. Both B and Hf are very good radiation absorbers, which is why they can be used as moderator rods in a variety of nuclear fission reactos [119]. This would add a minor radiation-shielding effect to the deployed material. The boron isotope B^{10} can decay into Li and He after neutron irradiation, following: $B^{10} + n^1 \rightarrow Li^7 + He^4$. The insoluble Helium is well known to form bubbles within metals, which leads to degradation of mechanical properties, swelling and structural disintegration [120]. However, considering the application in a nuclear fusion reactor, this rare occasion of B decay is expected to have a minor impact, compared to the continuous bombardment with He ions from the fusion reaction. Nevertheless, one has to take into account that in such a case, the positive effect of B on GB cohesion and mechanical properties is potentially lost over time.

5. Conclusion

In this work, ufg W samples doped with various interstitial and solute elements have been successfully fabricated. While the doping elements seem to only have little influence on grain size and hardness of the bulk material, a clear effect on the bending properties has been discovered utilizing microcantilever bending experiments. While the addition of C and Re seems to have a negative or hardly any effect on the mechanical properties of ufg tungsten, B and Hf serve to improve the mechanical performance and expended plastic energy density. It was demonstrated that B strengthens the GBs in tungsten directly (by enhancing GB cohesion) and also potentially indirectly (by replacing oxygen at the GB), which leads to an increase in bending strength, while maintaining the bending ductility level of the undoped ufg W. The strength of the boron doped tungsten can be increased even further by a heat treatment, leading to more segregation of B at GBs as well as an additional hardening-by-annealing effect. Hafnium, on the other hand, is not known to strengthen the GB directly, but

it is very effective in binding oxygen from them, leading to an improvement in bending strength and ductility. Due to the clear enhancement in GB cohesion and the close interlink of ductility and fracture toughness, it is assumed that the fracture toughness of ufg W also improves tremendously with the addition of B and Hf. Fracture mechanical tests to assess this expectation are planned and subject of future work.

In conclusion, it was demonstrated that the mechanical properties of ufg tungsten can be enhanced by the addition of suitable GB strengthening doping elements, such as B and Hf. These findings should also relate towards improving properties of coarser-grained tungsten material. However, once the fracture mode changes from intercrystalline to transcrystalline, no further increase in ductility and toughness through GB doping can be expected, as then the inherent brittleness of the tungsten crystal rather than the grain boundaries is the limiting factor. Therefore, it is recommended to combine the GBSE approach with very small grain sizes first and foremost, to fully tap the strengthening and toughening potential and create a high-performance material suitable to deploy in extreme environments.

Declaration of Competing Interest

The authors declare that they have no known competing financial interests or personal relationships that could have appeared to influence the work reported in this paper.

Acknowledgments

The authors acknowledge funding by the European Research Council under Grant number 771146 (MW, SD, DK). The authors thank Dr. Wolfram Knabl, Dr. Judith Köstenbauer and Plansee SE for providing tungsten material powder and support with sample annealing.

References

[1] R.O. Ritchie, The conflicts between strength and toughness, Nat. Mater. 10 (2011) 817–822, doi:10.1038/nmat3115.
[2] M.A. Meyers, A. Mishra, D.J. Benson, Mechanical properties of nanocrystalline materials, Prog. Mater. Sci. 51 (2006) 427–556, doi:10.1016/j.pmatsci.2005.08.003.
[3] C.C. Koch, D.G. Morris, K. Lu, A. Inoue, Ductility of nanostructured materials, MRS Bull. 24 (1999) 54–58, doi:10.1557/S0883769400051551.
[4] Y. Wang, M. Chen, F. Zhou, E. Ma, High tensile ductility in a nanostructured metal, Nature 419 (2002) 912–915, doi:10.1038/nature01133.
[5] E. Ma, Eight routes to improve the tensile ductility of bulk nanostructured metals and alloys, Jom 58 (2006) 49–53, doi:10.1007/s11837-006-0215-5.
[6] Y. Wei, Y. Li, L. Zhu, Y. Liu, X. Lei, G. Wang, Y. Wu, Z. Mi, J. Liu, H. Wang, H. Gao, Evading the strength-ductility trade-off dilemma in steel through gradient hierarchical nanotwins, Nat. Commun. 5 (2014), doi:10.1038/ncomms4580.
[7] E. Ma, T. Zhu, Towards strength–ductility synergy through the design of heterogeneous nanostructures in metals, Mater. Today. 20 (2017) 323–331, doi:10.1016/j.mattod.2017.02.003.
[8] Q. Wei, K.T. Ramesh, L.J. Kecskes, S.N. Mathaudhu, K.T. Hartwig, Ultrafine and Nanostructured Refractory Metals Processed by SPD : Microstructure and Mechanical Properties, Mater. Sci. Forum 579 (2008) 75–90, doi:10.4028/www.scientific.net/MSF.579.75.
[9] S. Shahrezaei, Y. Sun, S.N. Mathaudhu, Strength-ductility modulation via surface severe plastic deformation and annealing, Mater. Sci. Eng. A. 761 (2019) 138023, doi:10.1016/j.msea.2019.06.033.
[10] S.N. Mathaudhu, J A, K.T. Hartwig, L.J. Kecskes, Microstructures and recrystallization behavior of severely hot-deformed tungsten, Mater. Sci. Eng. A. 503 (2009) 28–31, doi:10.1016/j.msea.2008.03.051.
[11] N.A. Mara, D. Bhattacharyya, P. Dickerson, R.G. Hoagland, A. Misra, Ultrahigh strength and ductility of Cu-Nb nanolayered composites, Mater. Sci. Forum. 633–634 (2010) 647–653, doi:10.4028/www.scientific.net/MSF.633-634.647.
[12] A. Khalajhedayati, Z. Pan, T.J. Rupert, Manipulating the interfacial structure of nanomaterials to achieve a unique combination of strength and ductility, Nat. Commun. 7 (2016), doi:10.1038/ncomms10802.
[13] Z. Pan, T.J. Rupert, Amorphous intergranular films as toughening structural features, Acta Mater 89 (2015) 205–214, doi:10.1016/j.actamat.2015.02.012.
[14] E.O. Hall, The deformation and ageing of mild steel: III discussion of results, Proc. Phys. Soc. 64 (1951) 747–753.
[15] N.J. Petch, The cleavage strength of polycrystals, J. Iron Steel Inst. 174 (1953) 25–28.
[16] N.J. Petch, The ductile-brittle transition in the fracture of α-iron: I, Philos. Mag. 3 (1958) 1089–1097, doi:10.1080/14786435808237038.
[17] T. Hanamura, F. Yin, K. Nagai, Ductile-brittle transition temperature of ultrafine ferrite/cementite microstructure in a low carbon steel controlled by effective grain size, ISIJ Int 44 (2004) 610–617, doi:10.2355/isijinternational.44.610.
[18] A. Hohenwarter, R. Pippan, Fracture and fracture toughness of nanopolycrystalline metals produced by severe plastic deformation, Philos. Trans. R. Soc. A. 373 (2015) 20140366, doi:10.1098/rsta.2014.0366.
[19] A.V Sergueeva, N.A. Mara, A.K. Mukherjee, Plasticity at really diminished length scales, Mater. Sci. Eng. A. 463 (2007) 8–13, doi:10.1016/j.msea.2006.07.152.
[20] I.A. Ovid'Ko, A.G. Sheinerman, Kinetics of grain boundary sliding and rotational deformation in nanocrystalline materials, Rev. Adv. Mater. Sci. 35 (2013) 48–58.
[21] S.V. Bobylev, N.F. Morozov, I.A. Ovid'ko, Cooperative grain boundary sliding and migration process in nanocrystalline solids, Phys. Rev. Lett. 105 (2010) 055504, doi:10.1103/PhysRevLett.105.055504.
[22] H. Van Swygenhoven, P.M. Derlet, Grain-boundary sliding in nanocrystalline FCC metals, Phys. Rev. B - Condens. Matter Mater. Phys. 64 (2001) 224105, doi:10.1103/PhysRevB.64.224105.
[23] R. Pippan, A. Hohenwarter, The importance of fracture toughness in ultrafine and nanocrystalline bulk materials, Mater. Res. Lett. 4 (2016) 127–136, doi:10.1080/21663831.2016.1166403.
[24] D. Raabe, M. Herbig, S. Sandlöbes, Y. Li, D. Tytko, M. Kuzmina, D. Ponge, P. Choi, Grain boundary segregation engineering in metallic alloys: a pathway to the design of interfaces, Curr. Opin. Solid State Mater. Sci. 18 (2014) 253–261.
[25] M.A. Gibson, C.A. Schuh, Segregation-induced changes in grain boundary cohesion and embrittlement in binary alloys, Acta Mater 95 (2015) 145–155, doi:10.1016/j.actamat.2015.05.004.
[26] P. Lejcek, M. Šob, V. Paidar, Interfacial segregation and grain boundary embrittlement : An overview and critical assessment of experimental data and calculated results, Prog. Mater. Sci. 87 (2017) 83–139, doi:10.1016/j.pmatsci.2016.11.001.
[27] M. Kuzmina, D. Ponge, D. Raabe, Grain boundary segregation engineering and austenite reversion turn embrittlement into toughness : example of a 9 wt .% medium Mn steel, Acta Mater. 86 (2015) 182–192, doi:10.1016/j.actamat.2014.12.021.
[28] J. Bok, J. Wung, Z. Li, J. Chan, J. Gi, D. Raabe, H. Seop, Boron doped ultrastrong and ductile high-entropy alloys, Acta Mater 151 (2018) 366–376, doi:10.1016/j.actamat.2018.04.004.
[29] X. Wu, Y. You, X. Kong, J. Chen, G. Luo, G. Lu, C.S. Liu, Z. Wang, First-principles determination of grain boundary strengthening in tungsten : dependence on grain boundary structure and metallic radius of solute, Acta Mater 120 (2016) 315–326, doi:10.1016/j.actamat.2016.08.048.
[30] K. Leitner (née Babinsky), P.J. Felfer, D. Holec, J.M. Cairney, W. Knabl, A. Lorich, H. Clemens, S. Primig, On grain boundary segregation in molybdenum materials, Mater. Des. 135 (2017) 204–212, doi:10.1016/j.matdes.2017.09.019.
[31] K. Leitner, D. Scheiber, S. Jakob, S. Primig, H. Clemens, E. Povoden-Karadeniz, L. Romaner, How grain boundary chemistry controls the fracture mode of molybdenum, Mater. Des. 142 (2018) 36–43, doi:10.1016/j.matdes.2018.01.012.
[32] K. Leitner (née Babinsky), D. Lutz, W. Knabl, M. Eidenberger-Schober, K. Huber, A. Lorich, H. Clemens, V. Maier-Kiener, Grain boundary segregation engineering in as-sintered molybdenum for improved ductility, Scr. Mater. 156 (2018) 60–63, doi:10.1016/j.scriptamat.2018.07.008.
[33] S. Jakob, A. Hohenwarter, A. Lorich, W. Knabl, R. Pippan, H. Clemens, V. Maier-Kiener, Assessment of grain boundary cohesion of technically pure and boron micro-doped molybdenum via meso-scale three-point-bending experiments, Mater. Des. 207 (2021) 109848, doi:10.1016/j.matdes.2021.109848.
[34] S.C. Pun, W. Wang, A. Khalajhedayati, J.D. Schuler, J.R. Trelewicz, T.J. Rupert, Nanocrystalline Al-Mg with extreme strength due to grain boundary doping, Mater. Sci. Eng. A. 696 (2017) 400–406, doi:10.1016/j.msea.2017.04.095.
[35] H. Lee, V. Tomar, An examination of nickel doping effect on the mechanical strength of a tungsten grain boundary, Comput. Mater. Sci. 77 (2013) 131–138, doi:10.1016/j.commatsci.2013.04.034.
[36] R. Wu, A.J. Freeman, G.B. Olson, First principles determination of the effects of phosphorus and boron on iron grain boundary cohesion, Science (80-.) 265 (2006) 376–380, doi:10.1126/science.265.5170.376.
[37] P. Lejcek, Grain Boundary Segregation in Metals, Springer, Berlin-Heidelberg, 2010, doi:10.1016/0168-583X(93)95111-H.
[38] D. Scheiber, R. Pippan, P. Puschnig, L. Romaner, Ab initio search for cohesion-enhancing impurity elements at grain boundaries in molybdenum and tungsten, Model. Simul. Mater. Sci. Eng. 24 (2016) 85009, doi:10.1088/0965-0393/24/8/085009.
[39] D. Scheiber, R. Pippan, P. Puschnig, A. Ruban, L. Romaner, Ab-initio search for cohesion-enhancing solute elements at grain boundaries in molybdenum and tungsten, Int. J. Refract. Met. Hard Mater. 60 (2016) 75–81, doi:10.1016/j.ijrmhm.2016.07.003.
[40] W. Setyawan, R.J. Kurtz, Grain boundary strengthening properties of tungsten alloys, 2012. https://www.osti.gov/biblio/1055406.
[41] V.I. Razumovskiy, S.V. Divinski, L. Romaner, Solute segregation in Cu: DFT vs. Experiment, Acta Mater 147 (2018) 122–132, doi:10.1016/j.actamat.2018.01.011.

[42] V.I. Razumovskiy, A.Y. Lozovoi, I.M. Razumovskii, First-principles-aided design of a new Ni-base superalloy : influence of transition metal alloying elements on grain boundary and bulk cohesion, Acta Mater. 82 (2015) 369–377, doi:10.1016/j.actamat.2014.08.047.
[43] L. Huber, M. Militzer, Atomistic simulations of the interaction of alloying elements with grain boundaries in Mg, Acta Mater. 80 (2014) 194–204, doi:10.1016/j.actamat.2014.07.047.
[44] A.S. Ebner, S. Jakob, H. Clemens, R. Pippan, V. Maier-Kiener, S. He, W. Ecker, D. Scheiber, V.I. Razumovskiy, Grain boundary segregation in Ni-base alloys: a combined atom probe tomography and first principles study, Acta Mater. 221 (2021) 117354, doi:10.1016/j.actamat.2021.117354.
[45] M. Rieth, D.E.J. Armstrong, B. Dafferner, S. Heger, A. Hoffmann, M. Hoffmann, U. Jäntsch, M. Rohde, T. Scherer, V. Widak, H. Zimmermann, Tungsten as a structural divertor material, Adv. Sci. Technol. 73 (2010) 11–21, doi:10.4028/www.scientific.net/AST.73.11.
[46] S. Wurster, N. Baluc, M. Battabyal, T. Crosby, J. Du, C. Garcia-Rosales, A. Hasegawa, A. Hoffmann, A. Kimura, H. Kurishita, R.J. Kurtz, H. Li, S. Noh, J. Reiser, J. Riesch, M. Rieth, W. Setyawan, M. Walter, J.-H. You, R. Pippan, Recent progress in R&D on tungsten alloys for divertor structural and plasma facing materials, J. Nucl. Mater. 442 (2013) 181–189.
[47] M. Rieth, S.L. Dudarev, S.M.G. De Vicente, J. Aktaa, T. Ahlgren, S. Antusch, D.E.J. Armstrong, M. Balden, N. Baluc, M. Barthe, W..W. Basuki, M. Battabyal, C.S. Becquart, D. Blagoeva, H. Boldyryeva, J. Brinkmann, M. Celino, L. Ciupinski, J.B. Correia, A. De Backer, C. Domain, E. Gaganidze, C. Garcia-Rosales, J. Gibson, M.R. Gilbert, S. Giusepponi, B. Gludovatz, H. Greuner, K. Heinola, T. Höschen, A. Hoffmann, N. Holstein, F. Koch, W. Krauss, H. Li, S. Lindig, J. Linke, C. Linsmeier, P. López-ruiz, H. Maier, J. Matejicek, T.P. Mishra, M. Walter, T. Weber, T. Weitkamp, S. Wurster, M.A. Yar, J.H. You, A. Zivelonghi, Recent progress in research on tungsten materials for nuclear fusion applications in Europe, J. Nucl. Mater. 432 (2013) 482–500, doi:10.1016/j.jnucmat.2012.08.018.
[48] M. Rieth, S.L. Dudarev, S.M.G. De Vicente, J. Aktaa, T. Ahlgren, S. Antusch, D.E.J. Armstrong, M. Balden, N. Baluc, M. Barthe, W.W. Basuki, M. Battabyal, C.S. Becquart, D. Blagoeva, H. Boldyryeva, J. Brinkmann, M. Celino, L. Ciupinski, J.B. Correia, A. De Backer, C. Domain, E. Gaganidze, C. Garcia-rosales, J. Gibson, M.R. Gilbert, S. Giusepponi, B. Gludovatz, H. Greuner, K. Heinola, T. Höschen, A. Hoffmann, N. Holstein, F. Koch, W. Krauss, H. Li, S. Lindig, J. Linke, C. Linsmeier, P. Lopez-ruiz, H. Maier, J. Matejicek, T.P. Mishra, M. Muhammed, A. Munoz, M. Muzyk, K. Nordlund, D. Nguyen-manh, J. Opschoor, N. Ordas, M. Walter, T. Weber, T. Weitkamp, S. Wurster, M.A. Yar, J.H. You, A. Zivelonghi, A brief summary of the progress on the EFDA tungsten materials program, J. Nucl. Mater. 442 (2013) 173–180, doi:10.1016/j.jnucmat.2013.03.062.
[49] C. Ren, Z.Z. Fang, M. Koopman, B. Butler, J. Paramore, S. Middlemas, Methods for improving ductility of tungsten - A review, Int. J. Refract. Metals Hard Mater. 75 (2018) 170–183, doi:10.1016/j.ijrmhm.2018.04.012.
[50] D.E.J. Armstrong, X. Yi, E.A. Marquis, S.G. Roberts, Hardening of self ion implanted tungsten and tungsten 5-wt % rhenium, J. Nucl. Mater. 432 (2013) 428–436, doi:10.1016/j.jnucmat.2012.07.044.
[51] A. Xu, C. Beck, D.E.J. Armstrong, K. Rajan, G.D.W. Smith, P.A.J. Bagot, S.G. Roberts, Ion-irradiation-induced clustering in W – Re and W – Re – Os alloys : A comparative study using atom probe tomography and nanoindentation measurements, Acta Mater 87 (2015) 121–127, doi:10.1016/j.actamat.2014.12.049.
[52] D.E.J. Armstrong, P.D. Edmondson, S.G. Roberts, Effects of sequential tungsten and helium ion implantation on nano-indentation hardness of tungsten, Appl. Phys. Lett. 102 (2013) 251901.
[53] B. Gludovatz, S. Wurster, A. Hoffmann, R. Pippan, Fracture toughness of polycrystalline tungsten alloys, Int . J. Refract. Met. Hard Mater. 28 (2010) 674–678, doi:10.1016/j.ijrmhm.2010.04.007.
[54] J.S. Weaver, C. Sun, Y. Wang, S.R. Kalidindi, R.P. Doerner, N.A. Mara, S. Pathak, Quantifying the mechanical effects of He, W and He + W ion irradiation on tungsten with spherical nanoindentation, J. Mater. Sci. 53 (2018) 5296–5316, doi:10.1007/s10853-017-1833-8.
[55] B. Gludovatz, S. Wurster, A. Hoffmann, R. Pippan, A study into the crack propagation resistance of pure tungsten, Eng. Fract. Mech. 100 (2013) 76–85, doi:10.1016/j.engfracmech.2012.07.021.
[56] X. Zhang, K. Hattar, Y. Chen, L. Shao, J. Li, C. Sun, K. Yu, N. Li, M.L. Taheri, H. Wang, J. Wang, M. Nastasi, Radiation damage in nanostructured materials, Prog. Mater. Sci. 96 (2018) 217–321, doi:10.1016/j.pmatsci.2018.03.002.
[57] S. Wurster, R. Pippan, Nanostructured metals under irradiation, Scr. Mater. 60 (2009) 1083–1087, doi:10.1016/j.scriptamat.2009.01.011.
[58] I.J. Beyerlein, A. Caro, M.J. Demkowicz, N.A. Mara, A. Misra, B.P. Uberuaga, Radiation damage tolerant nanomaterials, Mater. Today. 16 (2013) 443–449, doi:10.1016/j.mattod.2013.10.019.
[59] I.J. Beyerlein, M.J. Demkowicz, A. Misra, B.P. Uberuaga, Defect-interface interactions, Prog. Mater. Sci. 74 (2015) 125–210, doi:10.1016/j.pmatsci.2015.02.001.
[60] M. Wurmshuber, D. Frazer, A. Bachmaier, Y. Wang, P. Hosemann, D. Kiener, Impact of interfaces on the radiation response and underlying defect recovery mechanisms in nanostructured Cu-Fe-Ag, Mater. Des. 160 (2018) 1148–1157, doi:10.1016/j.matdes.2018.11.007.
[61] W. Han, M.J. Demkowicz, N.A. Mara, E.G. Fu, S. Sinha, A.D. Rollett, Y. Wang, J.S. Carpenter, I.J. Beyerlein, A. Misra, Design of radiation tolerant materials via interface engineering, Adv. Mater. 25 (2013) 6975–6979, doi:10.1002/adma.201303400.
[62] W.S. Cunningham, K. Hattar, Y. Zhu, D.J. Edwards, J.R. Trelewicz, Suppressing irradiation induced grain growth and defect accumulation in nanocrystalline tungsten through grain boundary doping, Acta Mater. 206 (2021) 116629, doi:10.1016/j.actamat.2021.116629.
[63] O. El-Atwani, J.A. Hinks, G. Greaves, J.P. Allain, S.A. Maloy, Grain size threshold for enhanced irradiation resistance in nanocrystalline and ultrafine tungsten, Mater. Res. Lett. 5 (2017) 343–349, doi:10.1080/21663831.2017.1292326.
[64] O. El-Atwani, J.E. Nathaniel, A.C. Leff, B. Muntifering, J.K. Baldwin, K. Hattar, M.L. Taheri, The role of grain size in He bubble formation: Implications for swelling resistance, J. Nucl. Mater. 484 (2017) 236–244, doi:10.1016/j.jnucmat.2016.12.003.
[65] O. El-Atwani, S. Gonderman, M. Efe, G. De Temmerman, T. Morgan, K. Bystrov, D. Klenosky, T. Qiu, J.P. Allain, Ultrafine tungsten as a plasma-facing component in fusion devices: Effect of high flux, high fluence low energy helium irradiation, Nucl. Fusion. 54 (2014), doi:10.1088/0029-5515/54/8/083013.
[66] O. El-Atwani, J.A. Hinks, G. Greaves, S. Gonderman, T. Qiu, M. Efe, J.P. Allain, In-situ TEM observation of the response of ultrafine- and nanocrystalline-grained tungsten to extreme irradiation environments, Sci. Rep. 4 (2014) 4–10, doi:10.1038/srep04716.
[67] M. Wurmshuber, D. Frazer, M. Balooch, I. Issa, A. Bachmaier, P. Hosemann, D. Kiener, The effect of grain size on bubble formation and evolution in helium-irradiated Cu-Fe-Ag, Mater. Charact. 171 (2021) 110822, doi:10.1016/j.matchar.2020.110822.
[68] E. Smiti, P. Jouffrey, A. Kobylanski, The influence of carbon and oxygen in the grain boundary on the brittle-ductile transition temperature of tungsten bi-crystals, Scr. Metall. 18 (1984) 673–676.
[69] M. Wurmshuber, S. Doppermann, S. Wurster, D. Kiener, Ultrafine-grained tungsten by high-pressure torsion – bulk precursor versus powder processing route, IOP Conf. Ser. Mater. Sci. Eng. 580 (2019) 012051, doi:10.1088/1757-899X/580/1/012051.
[70] R. Pippan, S. Scheriau, A. Hohenwarter, M. Hafok, Advantages and limitations of HPT: a review, Mater. Sci. Forum. 584–586 (2008) 16–21, doi:10.4028/www.scientific.net/MSF.584-586.16.
[71] K. Babinsky, R. De Kloe, H. Clemens, S. Primig, A novel approach for site-specific atom probe specimen preparation by focused ion beam and transmission electron backscatter diffraction, Ultramicroscopy 144 (2014) 9–18, doi:10.1016/j.ultramic.2014.04.003.
[72] V. Maier, K. Durst, J. Mueller, B. Backes, H.W. Höppel, M. Göken, Nanoindentation strain-rate jump tests for determining the local strain-rate sensitivity in nanocrystalline Ni and ultrafine-grained Al, J. Mater. Res. 26 (2011) 1421–1430, doi:10.1557/jmr.2011.156.
[73] V. Maier-Kiener, K. Durst, Advanced nanoindentation testing for studying strain-rate sensitivity and activation volume, Jom 69 (2017) 2246–2255, doi:10.1007/s11837-017-2536-y.
[74] D.S. Gianola, C. Eberl, Micro- and nanoscale tensile testing of materials, Jom 61 (2009) 24–35, doi:10.1007/s11837-009-0037-3.
[75] D. Kiener, C. Motz, G. Dehm, R. Pippan, Overview on established and novel FIB based miniaturized mechanical testing using in-situ SEM, Int. J. Mater. Res. 100 (2009) 1074–1087, doi:10.3139/146.110149.
[76] D. Kiener, W. Grosinger, G. Dehm, R. Pippan, A further step towards an understanding of size-dependent crystal plasticity: in situ tension experiments of miniaturized single-crystal copper samples, Acta Mater 56 (2008) 580–592, doi:10.1016/j.actamat.2007.10.015.
[77] D. Kiener, A.M. Minor, Source truncation and exhaustion: insights from quantitative in situ TEM tensile testing, Nano Lett 11 (2011) 3816–3820, doi:10.1021/nl201890s.
[78] R. Wheeler, P.A. Shade, M.D. Uchic, Insights gained through image analysis during in situ micromechanical experiments, JOM 64 (2012) 58–65, doi:10.1007/s11837-011-0224-x.
[79] H.T. Vo, A. Reichardt, D. Frazer, N. Bailey, P. Chou, P. Hosemann, In situ microtensile testing on proton beam-irradiated stainless steel, J. Nucl. Mater. 493 (2017) 336–342, doi:10.1016/j.jnucmat.2017.06.026.
[80] M. Alfreider, M. Meindlhumer, V. Maier-Kiener, A. Hohenwarter, D. Kiener, Extracting information from noisy data: strain mapping during dynamic in situ SEM experiments, J. Mater. Res. 36 (2021) 2291–2304, doi:10.1557/s43578-020-00041-0.
[81] C. Motz, T. Schöberl, R. Pippan, Mechanical properties of micro-sized copper bending beams machined by the focused ion beam technique, Acta Mater 53 (2005) 4269–4279, doi:10.1016/j.actamat.2005.05.036.
[82] M. Meindlhumer, Micromechanical characterization of self-organized Ti1-xAlxN nanolamellae: the influence of interface coherency and phase alteration on fracture behavior, Montanuniversität Leoben (2016).
[83] E. Carrera, G. Giunta, M. Petrolo, Beam Structures: Classical and Advanced Theories, John Wiley & Sons, 2011.
[84] H. Duschanek, P. Rogl, Critical assessment and thermodynamic calculation of the binary systemm boron-tungsten (B-W), J. Phase Equilibria. 16 (1995) 150–161, doi:10.1007/BF02664852.
[85] W.D. Klopp, Review of ductilizing of group VIA elements by rhenium and other solutes, NASA TN D-4955. (1968).
[86] G.M. Song, M. Science, P.O. Box, The microstructure and elevated temperature strength of tungsten-titanium carbide composite, J. Mater. Sci. 37 (2002) 3541–3548.
[87] C. Fan, C. Liu, F. Peng, N. Tan, M. Tang, Q. Zhang, Q. Wang, F. Li, J. Wang, Y. Chen, H. Liang, S. Guan, K. Yang, J. Liu, Phase stability and incompressibility of tungsten boride (WB) researched by in-situ high pressure x-ray di ff

raction, Phys. B Phys. Condens. Matter. 521 (2017) 6–12, doi:10.1016/j.physb.2017.06.028.
[88] M. Thuvander, H.O. Andrén, PFIM studies of grain and phase boundaries: a review, Mater. Charact. 44 (2000) 87–100, doi:10.1016/S1044-5803(99)00052-2.
[89] B.W. Krakauer, D.N. Seidman, Absolute atomic-scale measurements of the Gibbsian interfacial excess of solute at internal interfaces, Phys. Rev. B. 48 (1993) 6724–6727, doi:10.1103/PhysRevB.48.6724.
[90] R.C. Koo, Recovery in cold-worked tungsten, J. Less-Common Met. 3 (1961) 412–428, doi:10.1016/0022-5088(61)90016-9.
[91] B. Sestak, A. Seeger, Gleitung und Verfestigung in kubisch-raumzentrierten Metallen, Zeitschrift Für Met 69 (1978), doi:10.1515/ijmr-1978-690401.
[92] A. Seeger, The temperature and strain-rate dependence of the flow stress of body-centred cubic metals: a theory based on kink-kink interactions, Zeitschrift Für Met 72 (1981) 369–380, doi:10.1515/ijmr-1981-720601.
[93] A. Argon, Strengthening Mechanisms in Crystal Plasticity, Oxford University Press, New York, 2008, doi:10.1093/acprof:oso/9780198516002.001.0001.
[94] D. Kiener, R. Fritz, M. Alfreider, A. Leitner, R. Pippan, V. Maier-Kiener, Rate limiting deformation mechanisms of BCC metals in confined volumes, Acta Mater 166 (2019) 687–701, doi:10.1016/J.ACTAMAT.2019.01.020.
[95] D. Wu, X.L. Wang, T.G. Nieh, Variation of strain rate sensitivity with grain size in Cr and other body-centred cubic metals, J. Phys. D. Appl. Phys. 47 (2014), doi:10.1088/0022-3727/47/17/175303.
[96] B.D. Beake, A.J. Harris, J. Moghal, D.E.J. Armstrong, Temperature dependence of strain rate sensitivity, indentation size effects and pile-up in polycrystalline tungsten from 25 to 950 °C, Mater. Des. 156 (2018) 278–286, doi:10.1016/j.matdes.2018.06.063.
[97] J. Kappacher, A. Leitner, D. Kiener, H. Clemens, V. Maier-Kiener, Thermally activated deformation mechanisms and solid solution softening in W-Re alloys investigated via high temperature nanoindentation, Mater. Des. 189 (2020) 108499, doi:10.1016/j.matdes.2020.108499.
[98] L. Romaner, C. Ambrosch-Draxl, R. Pippan, Effect of rhenium on the dislocation core structure in tungsten, Phys. Rev. Lett. 104 (2010) 195503, doi:10.1103/PhysRevLett.104.195503.
[99] A. Hohenwarter, R. Pippan, Anisotropic fracture behavior of ultrafine-grained iron, Mater. Sci. Eng. A. 527 (2010) 2649–2656, doi:10.1016/j.msea.2009.12.033.
[100] S. Wurster, B. Gludovatz, A. Hoffmann, R. Pippan, Fracture behavior of tungsten-vanadium and tungsten-tantalum alloys and composites, J. Nucl. Mater. 413 (2011) 166–176, doi:10.1016/j.jnucmat.2011.04.025.
[101] J. Reiser, J. Hoffmann, U. Jäntsch, M. Klimenkov, S. Bonk, C. Bonnekoh, A. Hoffmann, T. Mrotzek, M. Rieth, Ductilisation of tungsten (W): On the increase of strength AND room-temperature tensile ductility through cold-rolling, Int. J. Refract. Met. Hard Mater. 64 (2017) 261–278, doi:10.1016/j.ijrmhm.2016.10.018.
[102] N. Fonstein, Advanced High Strength Sheet Steels, Springer International Publishing, 2015, doi:10.1007/978-3-319-19165-2.
[103] P. Khedkar, R. Motagi, P. Mahajan, G. Makwana, A review on advance high strength steels, Int. J. Curr. Eng. Technol. 6 (2016) 240–243 https://inpressco.com/wp-content/uploads/2016/10/Paper53240-243.pdf.
[104] Q. Wei, T. Jiao, K.T. Ramesh, E. Ma, L.J. Kecskes, L. Magness, R. Dowding, V.U. Kazykhanov, R.Z. Valiev, Mechanical behavior and dynamic failure of high-strength ultrafine grained tungsten under uniaxial compression, Acta M 54 (2006) 77–87, doi:10.1016/j.actamat.2005.08.031.
[105] X. Huang, N. Hansen, N. Tsuji, Hardening by annealing and softening by deformation in nanostructured metals, Science (80-.) 312 (2006) 249–251.
[106] O. Renk, A. Hohenwarter, K. Eder, K.S. Kormout, J.M. Cairney, R. Pippan, Increasing the strength of nanocrystalline steels by annealing: Is segregation necessary? Scr. Mater. 95 (2015) 27–30, doi:10.1016/j.scriptamat.2014.09.023.
[107] T.J. Rupert, J.R. Trelewicz, C.A. Schuh, Grain boundary relaxation strengthening of nanocrystalline Ni-W alloys, J. Mater. Res. 27 (2012) 1285–1294, doi:10.1557/jmr.2012.55.
[108] J. Hu, Y.N. Shi, X. Sauvage, G. Sha, K. Lu, Grain boundary stability governs hardening and softening in extremely fine nanograined metals, Science (80-.) 355 (2017) 1292–1296, doi:10.1126/science.aal5166.
[109] M. Alfreider, I. Issa, O. Renk, D. Kiener, Probing defect relaxation in ultra-fine grained Ta using micromechanical spectroscopy, Acta Mater 185 (2020) 309–319, doi:10.1016/j.actamat.2019.12.011.
[110] H. Van Swygenhoven, J.R. Weertman, Deformation in nanocrystalline metals, Mater. Today. 9 (2006) 24–31, doi:10.1016/S1369-7021(06)71494-8.
[111] H. Van Swygenhoven, Footprints of plastic deformation in nanocrystalline metals, Mater. Sci. Eng. A. 483–484 (2008) 33–39, doi:10.1016/j.msea.2006.10.204.
[112] L.E. Murr, Dislocation ledge sources: dispelling the myth of frank–read source importance, Metall. Mater. Trans. A Phys. Metall. Mater. Sci. 47 (2016) 5811–5826, doi:10.1007/s11661-015-3286-5.
[113] V. Turlo, T.J. Rupert, Grain boundary complexions and the strength of nanocrystalline metals: Dislocation emission and propagation, Acta Mater 151 (2018) 100–111, doi:10.1016/j.actamat.2018.03.055.
[114] M.A. Tschopp, G.J. Tucker, D.L. McDowell, Atomistic simulations of tension-compression asymmetry in dislocation nucleation for copper grain boundaries, Comput. Mater. Sci. 44 (2008) 351–362, doi:10.1016/j.commatsci.2008.03.041.
[115] B. Lüthi, L. Ventelon, C. Elsässer, D. Rodney, F. Willaime, First principles investigation of carbon-screw dislocation interactions in body-centered cubic metals, Model. Simul. Mater. Sci. Eng. 25 (2017) 84001, doi:10.1088/1361-651X/aa88eb.
[116] B. Lüthi, F. Berthier, L. Ventelon, B. Legrand, D. Rodney, F. Willaime, Ab initio thermodynamics of carbon segregation on dislocation cores in bcc iron, Model. Simul. Mater. Sci. Eng. 27 (2019), doi:10.1088/1361-651X/ab28d4.
[117] L. Ventelon, B. Lüthi, E. Clouet, L. Proville, B. Legrand, D. Rodney, F. Willaime, Dislocation core reconstruction induced by carbon segregation in bcc iron, Phys. Rev. B - Condens. Matter Mater. Phys. 91 (2015) 1–5, doi:10.1103/PhysRevB.91.220102.
[118] J. Qian, C.Y. Wu, J.L. Fan, H.R. Gong, Effect of alloying elements on stacking fault energy and ductility of tungsten, J. Alloys Compd. 737 (2018) 372–376, doi:10.1016/j.jallcom.2017.12.042.
[119] K.L. Murty, I. Charit, An Introduction to Nuclear Materials: Fundamentals and Applications, WILEY-VCH, Weinheim, 2013 https://books.google.com/books?id=wRVwAAAAQBAJ&pgis=1.
[120] M. Wurmshuber, M. Balooch, X. Huang, P. Hosemann, D. Kiener, Helium-induced swelling and mechanical property degradation in ultrafine-grained W and W-Cu nanocomposites for fusion applications, Scr. Mater. 213 (2022) 114641, doi:10.1016/j.scriptamat.2022.114641.